





Cite this: *J. Mater. Chem. A*, 2021, 9, 5542Unravelling moisture-induced CO₂ chemisorption mechanisms in amine-modified sorbents at the molecular scale†Mariana Sardo, ^a Rui Afonso,^a Joanna Jużków,^a Marlene Pacheco,^b Marta Bordonhos, ^b Moisés L. Pinto,^b José R. B. Gomes ^a and Luís Mafrá ^{*a}

This work entails a comprehensive solid-state NMR and computational study of the influence of water and CO₂ partial pressures on the CO₂-adducts formed in amine-grafted silica sorbents. Our approach provides atomic level insights on hypothesised mechanisms for CO₂ capture under dry and wet conditions in a tightly controlled atmosphere. The method used for sample preparation avoids the use of liquid water slurries, as performed in previous studies, enabling a molecular level understanding, by NMR, of the influence of controlled amounts of water vapor (down to ca. 0.7 kPa) in CO₂ chemisorption processes. Details on the formation mechanism of moisture-induced CO₂ species are provided aiming to study CO₂ : H₂O binary mixtures in amine-grafted silica sorbents. The interconversion between distinct chemisorbed CO₂ species was quantitatively monitored by NMR under wet and dry conditions in silica sorbents grafted with amines possessing distinct bulkiness (primary and tertiary). Particular attention was given to two distinct carbonyl environments resonating at $\delta_C \sim 161$ and 155 ppm, as their presence and relative intensities are greatly affected by moisture depending on the experimental conditions. 1D and 2D NMR spectral assignments of both these ¹³C resonances were assisted by density functional theory calculations of ¹H and ¹³C chemical shifts on model structures of alkylamines grafted onto the silica surface that validated various hydrogen-bonded CO₂ species that may occur upon formation of bicarbonate, carbamic acid and alkylammonium carbamate ion pairs. Water is a key component in flue gas streams, playing a major role in CO₂ speciation, and this work extends the current knowledge on chemisorbed CO₂ structures and their stabilities under dry/wet conditions, on amine-modified solid surfaces.

Received 8th October 2020
Accepted 8th January 2021

DOI: 10.1039/d0ta09808f

rsc.li/materials-a

1. Introduction

General recognition of the environmental impact of large concentrations of CO₂ present in the atmosphere has continuously risen, leading to increased efforts to mitigate greenhouse effects.¹ In order to reduce CO₂ emissions, new solid adsorbent materials are actively being sought for capturing CO₂ from stationary sources with dilute CO₂ concentrations, in replacement of liquid-phase amine adsorbents, to overcome the inherent chemical degradation, low loading capacities, corrosion and low energy efficiency issues related to the use of aqueous amine solutions.^{2–7} Amine-based solid adsorbents have been extensively studied for carbon capture and storage (CCS)

and also shown to be good candidates for direct air capture (DAC) applications, involving extremely low CO₂ concentrations (ca. 400 ppm),¹ based on negative carbon emission technologies.

Combustion products from burning fossil fuels in air, and the resulting flue gas, typically contain low concentrations of CO₂ (<20%) and about 80% N₂. In both exhaust gases and air, moisture is a ubiquitous component and depending on the type of fuels and the combustion conditions, flue gas contains about 8–20% moisture (water vapor).⁸ For any large-scale real-world CO₂ capture or separation application, the effect of moisture on adsorbents must therefore be taken under consideration.

Assessing the type of chemisorbed CO₂ structure, under moist conditions, formed in such porous adsorbents with amines is therefore of paramount importance to design and optimise effective sorbents for CO₂/N₂ separation from industrial flue gas streams as well as CO₂/H₂ and CO₂/CH₄ separation processes. Despite numerous contributions, understanding the stability and chemical nature of these CO₂ species is not straightforward,⁹ due to the many variables (temperature, gas pressure, amine coverage, silanol density, pore textural

^aCICECO – Aveiro Institute of Materials, Department of Chemistry, University of Aveiro, Campus Universitário de Santiago, 3810-193 Aveiro, Portugal. E-mail: msardo@ua.pt; lmafra@ua.pt

^bCERENA, Instituto Superior Técnico, University of Lisbon, Av. Rovisco Pais, 1049-001 Lisboa, Portugal

† Electronic supplementary information (ESI) available. See DOI: 10.1039/d0ta09808f



properties) that may influence CO₂ speciation (not to mention the number of process variables that should also guide the adsorbent choice). Although CO₂-chemisorbent materials such as MOFs^{10–14}/postsynthetically modified MOFs^{15–17} or alkaline ceramics^{18,19} are emerging as potential candidates for CO₂ captors from wet gas mixtures, mesoporous silicas, such as SBA-15 functionalized with amines, reported in this work, are among the most relevant materials being developed^{2,4} due to their high selectivity, capacity towards dilute CO₂ sources and moisture tolerance.^{3,4,20}

The reaction mechanism and products, resulting from co-adsorption of CO₂ and moisture by silica supported amine adsorbents, may vary based on the type of amino groups, amine loading, moisture content and sometimes whether the amine is chemically grafted, physically impregnated on the support or a mixture of both.^{21–23} The role of water in the CO₂ capture efficiency is somewhat controversial because some authors claim that the presence of moisture enhances CO₂ adsorption capacity^{21,24} while others report no synergy effects between moisture and an increase of CO₂ adsorption capacity by amine-grafted solid sorbents.^{25–30} The enhancement of CO₂ capacity under moist conditions has been many times associated with the increase of amine efficiency (CO₂/N) from ~0.5 (dry) to 1 (wet) induced by the formation of bicarbonate species in the presence of water molecules.³¹ It is known that basic surface amines and acidic CO₂ molecules interact to form surface carbamate and carbamic acid species under anhydrous conditions and bicarbonate/carbonate species when water is present.^{3,4,32,33} Nevertheless, which CO₂ species is really contributing to increase CO₂ adsorption efficiency, under wet conditions, has been a subject of high interest.^{1,28,34,35} In fact, the increase of CO₂ capacity under humid conditions has been attributed, by some authors, to the formation of more carbamate species in the presence of humidity, rather than formation of bicarbonate species.^{1,28,34,35} Bacsik and co-workers²⁸ explained that water could induce disruption of amine H-bonds with neighbouring surface species thus increasing their accessibility to CO₂ molecules, leading to the formation of more ammonium carbamate ion pairs.

Differentiating moisture-induced CO₂ species (*e.g.*, bicarbonate) from carbamic acid or carbamates is a difficult task, mainly because the signals arising from carbamic acid and carbamate species often dominate the FTIR and NMR spectra. Several experimental studies detected bicarbonate species, mainly through FTIR spectroscopy, in aqueous amine solutions^{36,37} as well as on porous solids functionalized with amines.^{38–41} ¹³C solid-state NMR has been a valuable complementary method to identify surface bicarbonates in studies involving amine functionalized sorbents, but the assignment of CO₂ species is complicated due to ill-resolved spectra in the CO₂ chemisorption region. This is because of the ¹³C isotropic chemical shift (CS) overlap between resonances associated with different CO₂ species.^{34,42,43}

Recently, Foo and co-workers³⁸ hinted on the presence of bicarbonate ions on primary amine grafted-SBA-15 through a combined FTIR/NMR study. The existence of bicarbonate ions was attributed to the presence of residual physisorbed water on

the amine-grafted sample, exhibiting a resonance near 161 ppm in the ¹³C NMR spectrum. Overall, ammonium bicarbonate species have been previously assigned in the literature based on ¹³C NMR resonances appearing between 161 and 165 ppm,^{40,43–45} in tertiary amine-grafted mesoporous SBA-15, as a solid product of the reaction between NH₃ and CO₂ under humid conditions and in amine-modified COFs.⁴¹ However, the assignment of such species in tertiary amine-grafted SBA-15 was performed on samples without rigorous control of the CO₂ and H₂O partial pressures. This may lead to significant changes in the NMR spectra as shown in this work.

In this work, we present a comprehensive study involving the species formed upon CO₂ and H₂O adsorption on primary and tertiary amine-grafted SBA-15 (3-aminopropyltriethoxysilane (APTES) and [3-(diethylamino)propyl]trimethoxysilane (DEAPTES)). For that purpose, binary mixtures of ¹³C-labeled CO₂ (¹³CO₂) and water were used. A combined high-resolution ¹³C/¹H solid-state NMR and computational study is presented to access all the variables involving the formation of moisture-induced species. Although tertiary amines are not usually considered of practical relevance in carbon capture applications due to their low CO₂ uptake under dry conditions, they were used in this work since they are not expected to form the “dominant” alkylammonium carbamate species, thus facilitating the detection and assignment of signals arising from dilute CO₂ species. The method we explore is significantly different from previously reported methods,^{40,44} as all wet samples were prepared without the use of slurries, which may give rise to additional species formed by dissolution in water. Instead, our method consists in dosing, in a controlled environment, specific amounts of water and CO₂ partial pressures, as explained in detail in Section 3.3. Molecular models of the silica surface functionalized with amines engaged in different intermolecular interactions were assessed using DFT methods, whose results are compared with solid-state NMR evidence. This combination facilitates the assessment of computer models accuracy thus helping in the identification of the observed moisture-induced CO₂ species.

2. Methods

2.1. Materials preparation and characterization

SBA-15 (8 nm pore size) was purchased from Sigma-Aldrich and used without further purification. SBA-15 functionalization was carried out with amino-organosilanes; APTES (purity > 98%) and 3-DEAPTES (96%) were acquired from Sigma-Aldrich. It is worth mentioning that the dryness conditions of the reaction media and material are of paramount importance to prevent extension of lateral silane polymerization within the materials and to allow efficient silane functionalization. To achieve this, typically 2 g of SBA-15 was introduced in a closed reflux apparatus connected to a vacuum line and heated to 150 °C for 2 h. After cooling, nitrogen was introduced into the system prior to the opening of the reflux apparatus, and SBA-15 was refluxed with 100 cm³ of dry toluene (Aldrich, 99.8%) containing 9 mmol of the amino-organosilane for 24 h in a nitrogen atmosphere. The resulting material was purified by Soxhlet extraction with



dry toluene, to remove the unreacted amino-organosilanes, and finally dried under vacuum at 120 °C for 24 h. Functionalized materials were named APTES@SBA-15 and DEAPTES@SBA-15.

The thermogravimetric, differential scanning calorimetry experiments, elemental analysis as well as the porous texture characterization of the materials (*via* N₂ adsorption at −196 °C) were performed using the same protocol as described in our previous work⁴⁶ (details in the ESI†).

2.2. Sorption apparatus for loading samples with ¹³CO₂

The sorption apparatus (Scheme S1†) comprises a laboratory-made high-vacuum line, connected to a turbomolecular pumping station (HiCube 80, Pfeiffer Vacuum), capable of vacuum greater than 10^{−2} Pa. A borosilicate glass cell, adapted from the description in the literature, was connected to the vacuum line and served as an enclosure for an NMR rotor allowing the degassing and heating of zirconia NMR rotors up to 300 °C under high vacuum. The heating was performed with a laboratory-made oven connected to a power controller (Eurotherm 3116), and the temperature measured with a thermocouple. The desired gas was introduced into the system from the canister connected to the vacuum line and the cell. The pressure inside the cell was measured with a capacitance transducer (MKS Instruments, Baratron 722B).

All samples of APTES@SBA-15 and DEAPTES@SBA-15 were packed in zirconia NMR rotors, enclosed into the sorption apparatus and dried by degassing and heating (150 °C, 3 h, ramp of 2.5 °C min^{−1}) under vacuum (Scheme S1†). After cooling down under vacuum, ¹³CO₂ (Cortecnet, 99 atom% ¹³C; <3 atom% ¹⁸O) and water vapor (see Section 3.3 for further details) were introduced into the system up to the desired partial pressures and allowed to equilibrate for 4.5 h. Water vapor was introduced into the cell from a glass container with liquid water connected to the vacuum line by opening a valve on the glass container. Prior to use, deionized water (Millipore Milli-Q) was further purified by freeze–vacuum–thaw cycles. After adsorption of water vapor and CO₂ with the desired partial pressures, the cell was then filled with helium (Air Liquide, 99.999%), if needed, up to the atmospheric pressure. Finally, the NMR rotor was closed inside the cell and only then the cell was opened to remove the rotor for NMR measurements.

2.3. Computational details

The clusters used to model the silica surface are based on the experimental crystallographic structure of alpha-quartz⁴⁷ using the atomic positions of the silicon and oxygen atoms. Dangling bonds at the edges of the cluster models due to elimination of Si atoms were saturated with H atoms along the O–Si directions of the perfect crystal and imposing an O–H distance equal to 0.96 Å.⁴⁸ Note that although the real surface of mesoporous silicas is amorphous, using a surface built from a crystalline structure should not dramatically influence the results from the calculations, as we are dealing with relatively small clusters.

The silylpropylamines were grafted (through optimisation) on the clusters where OH groups existed, each binding three surface OH groups. Subsequent optimisations of different

species involved the relaxation of the alkyl chain (and the respective functional group at its end), water or CO₂ molecules (when present), the SiO₃ moieties binding the alkylamines, and the surface OH groups, while the remaining Si and O atoms were kept frozen at their crystallographic positions. The fixation of some atomic positions provides a simple but effective representation of the mechanical embedding of the solid covalent oxide surface.^{49,50} As common practice, several different initial conformations were studied (please refer to ref. 9 for additional details), with all discussions below considering only the most stable conformations of each kind. The absence of imaginary values in the vibrational modes involving the atoms optimised in the different structural models ensured that the structures are true minima on their potential energy surfaces.

The M06-2X hybrid functional of Truhlar and Zhao,^{51,52} based on the meta-generalized gradient approximation, and the standard 6-31G(d) basis set^{53,54} with a single polarisation function in all the atoms except hydrogen, as included in the Gaussian 09 software,⁵⁵ were used in all the structural optimisations, in the calculation of electronic energies or Gibbs energies at *T* = 298.15 K, and vibrational frequencies. In all calculations, the default integration grids and convergence thresholds in the Gaussian 09 software were employed.

NMR shielding tensors of the optimized geometries have been computed with the GIAO method,^{56,57} also using the M06-2X functional and the 6-31G(d) basis set. These conditions typically create relatively small root-mean-square errors of the calculated ¹³C chemical shifts (*cf.* 3.2 ppm).⁵⁸ The isotropic magnetic shielding tensors calculated for the clusters were subtracted from those calculated for gas-phase tetramethylsilane (at 0 ppm, as in our previous work^{4,9,20}).

The M06-2X functional has been the default choice in our work with amine-functionalised silicas,⁹ with calculated NMR and infrared values in excellent agreement with the experimental results. In fact, tests with larger basis sets, *e.g.* 6-31G(d,p), 6-31+G(d,p) or 6-311++G(d,p) were found to lead to systematic overestimations of the experimental ¹H and ¹³C shifts of the three carbon species reported in our previous work,⁴ when considering tetramethylsilane calculated at the same level of theory as the reference (Tables S4–S7 in the ESI†), with the overestimations increasing with the increase of the basis set size. These observations are aligned with those in other studies reported in the literature, where it was found that the increase of the basis set size from 6-31G(d) to 6-311G(2d,2p) or def2-TZVP^{54,59} did not lead to any visible increment in the accuracy of the calculated NMR shifts.^{4,9,20,56–58}

2.4. Solid-state NMR measurements

¹H, ²⁹Si, and ¹³C NMR spectra were acquired on a Bruker Avance III 400 and 700 spectrometers operating at *B*₀ fields of 9.4 and 16.4 T, respectively, with ¹H/²⁹Si/¹³C Larmor frequencies of 400.1/79.5/100.6 MHz and 700.1/139.1/176.1 MHz, respectively. All experiments were performed on a double-resonance 4 mm Bruker MAS probe. Samples were packed into ZrO₂ rotors with Kel-F caps. Spinning rates between 10



and 15 kHz were employed to record all the spectra (see figure captions for details). ^1H and ^{13}C CSs are quoted in ppm from TMS (0 ppm) and α -glycine (secondary reference, C=O at 176.03 ppm), respectively. ^{29}Si CSs were referenced with respect to the external secondary reference Q8M8 (octa(dime-thylsiloxy)silsesquioxane) setting the high frequency signal (left side resonance) to 11.5 ppm. ^1H single-pulse excitation magic angle spinning (MAS) NMR spectra were recorded at a spinning rate of 15 kHz using a pulse width of $2.66\ \mu\text{s}$ (90° flip angle) corresponding to a radio frequency (rf) field strength of *ca.* 94 kHz. A recycle delay (RD) of 8 s was found to be sufficient and used for all samples. The ^{13}C CPMAS spectra were acquired under the following experimental conditions: ^1H 90° pulse set to $3.0\ \mu\text{s}$ corresponding to an rf of $\sim 83\ \text{kHz}$; the CP step was performed with a contact time (CT) of $2000\ \mu\text{s}$ using a 70–100% RAMP shape at the ^1H channel and using a 50 kHz square shape pulse on the ^{13}C channel; RD was 5 s. During the acquisition, a SPINAL-64 decoupling scheme was employed using a pulse length for the basic decoupling units of $7\ \mu\text{s}$ at an rf field strength of 83 kHz. The ^1H – ^{13}C LG-CP HETCOR spectra were acquired using frequency-switched Lee–Goldburg (FSLG) ^1H homonuclear decoupling during the indirect dimension (t_1). For LG-CP the conditions used were CT of $2000\ \mu\text{s}$, ^{13}C rf amplitude ramped at 50–100%, and an rf amplitude for ^1H spin-lock of 50 kHz at an LG offset irradiation of $-50\ 000/\sqrt{2} = -35\ 354\ \text{Hz}$. 70 t_1 points with 1024 scans each were recorded along the indirect dimension. An ^1H rf field strength of 83 kHz and asymmetric LG offset of 54 925 Hz and $-62\ 925\ \text{Hz}$ were used for FSLG decoupling employing an LG pulse of $9.8\ \mu\text{s}$. The indirect dimension dwell time was set equal to four FSLG blocks ($78.4\ \mu\text{s}$). Quadrature detection in t_1 was achieved by the States-TPPI method. The ^1H CSs were corrected assuming a scaling factor of $1/\sqrt{3}$ for FSLG decoupling. The ^1H – ^{29}Si CP HETCOR spectra were acquired with CT of $8000\ \mu\text{s}$; ^{29}Si rf power amplitude ramped at 50–100% and an ^1H spin-lock rf amplitude of 50 kHz. 20 t_1 points with 3072 scans each were recorded along the indirect dimension. All reported ^1H NMR CSs extracted from the HETCOR spectra have an average estimated error of $\pm 0.5\ \text{ppm}$ due to the scaling factors used for FSLG decoupling to calibrate the ^1H CSs at the indirect dimension. Further relevant experimental details can be found in the corresponding figure captions. Fitting of the APTES@SBA-15 NMR spectra recorded at 12 kHz MAS was performed with DMFIT⁶⁰ software. Fitting errors were below 5%.

2.5. Adsorption of CO_2

The CO_2 (99.998%, Air Liquide) adsorption isotherms were collected at $25\ ^\circ\text{C}$ in increasing pressures up to *ca.* 1000 kPa (10 bar), using the manometric method. These experiments were performed in a lab-made stainless-steel volumetric apparatus with a pressure transducer (MKS, Baratron 627D14TBC1B), and equipped with a vacuum system (Pfeiffer Vacuum, HiCube 80) that achieves vacuum pressures better than $10^{-4}\ \text{Pa}$. Prior to collecting experimental data, all samples were degassed at $150\ ^\circ\text{C}$ for 2 h, at a vacuum pressure below $10^{-4}\ \text{Pa}$. During the

experiments, the temperature of the adsorption system and of each sample was controlled with a thermostatic water bath with an accuracy of $0.01\ ^\circ\text{C}$ (Julabo, MB-5). Experimental adsorption isotherms were calculated considering the non-ideality of the gas phase using the second and third virial coefficients. Additionally, the experimental excess adsorbed amounts were converted to the absolute adsorbed amounts by accounting the porous volume of the material and the density of the gas phase.

For the adsorption of CO_2 in samples with a known amount of preadsorbed water, a given pressure of water vapor was introduced in the calibrated volume (about 2.08 kPa) and allowed to equilibrate at room temperature. The value of the pressure was recorded and the vapor dosed to the freshly activated sample by the opening of the sample valve. After equilibration, the final pressure was below the sensitivity of the pressure transducer ($<6\ \text{Pa}$) and it was assumed that all water was adsorbed in the sample. For the calculations of the adsorbed amounts, the non-ideality of the water vapor was accounted with the second virial coefficient. Prior to use, the deionized water (Millipore Milli-Q) was further purified by freeze–vacuum–thaw cycles.

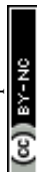
3. Results and discussion

3.1. Characterization of the adsorbent materials

The materials were first characterized to assess the porosity of the samples, thermal stability and amine content after functionalization with the amines. Textural properties of the studied porous samples were obtained by nitrogen adsorption isotherms (Fig. S1 and Table S1†). These data indicate an effective functionalization on the SBA-15 pores and are in agreement with those obtained in our previous work.⁴

The BET surface area of the parent sample (SBA-15) decreased from *ca.* 743 to 340 and $329\ \text{m}^2\ \text{g}^{-1}$ upon functionalization with APTES and DEAPTES, respectively. The pore volume also drops upon functionalization with both amines with a slightly higher decrease for the material functionalized with DEAPTES (bulkier amine). Further indications of the successful functionalization were given by the nitrogen content of the samples obtained by chemical analysis (Table S1†). The infrared spectra (Fig. S2†) show the typical Si–O stretching band at $\sim 1100\ \text{cm}^{-1}$ from silica, and additional vibrations in the regions of 3500 – $3300\ \text{cm}^{-1}$ (stretching of O–H/N–H bond) and 1650 – $1580\ \text{cm}^{-1}$ (O–H/N–H amine bending).

Thermal analysis of the samples by thermogravimetry (TGA) and differential scanning calorimetry (DSC) provides information on the stability of the samples with temperature, which is relevant to define the activation conditions for the samples. A first mass loss corresponding to an endothermic process is observed until about $120\ ^\circ\text{C}$ (Fig. S3†), attributed to the loss of water and other gases or solvents adsorbed on the sample. From about $230\ ^\circ\text{C}$ onwards, a second mass loss is observed on the samples functionalized with amines (absent in the parent SBA-15), which corresponds to the exothermic decomposition of the grafted amines. In fact, the mass loss between 150 and $500\ ^\circ\text{C}$ agrees with the amine content obtained from the chemical analysis; the amine content from TG data gives an estimation of



1.2 mmol g⁻¹ and 1.0 mmol g⁻¹ for APTES@SBA-15 and DEAPTES@SBA-15, respectively. Considering these results, the activation of the samples before adsorption and NMR studies was performed at 150 °C to ensure the proper cleaning of the surface without degrading the samples. These findings are in line with our previous studies^{4,20} and further confirm the presence of the amines on the surface of SBA-15.

The presence of amines in the samples was further confirmed by ¹³C ssNMR (Fig. S4†). Peaks with chemical shifts in the 60 to 0 ppm range were observed; APTES@SBA-15 presented three peaks at 8.7, 21.5 and 42.5 ppm corresponding to the propyl chain and DEAPTES@SBA-15 presented peaks at 9.6, 19.4, 46.2 and 56.7 ppm corresponding to the propyl chain and ethyl groups. These values agree with our previous results.⁴

3.2. Adsorption of CO₂ in dry and wet amine-functionalized silicas

The adsorption of CO₂ on the sample functionalized with primary amine (APTES@SBA-15) was carried out in the dry

sample and in the sample after pre-adsorption of 0.157 mmol g⁻¹ of water (Fig. 1, top). We opted to only use a small amount of water (low coverings) because we are interested in looking at the effect on the pore surface and not on the filling of the pores, when CO₂ is adsorbed. The results clearly show that the small amount of water at the surface does not have a noticeable effect on the CO₂ adsorption in all pressure ranges (up to 1000 kPa), since both isotherms overlap. Thus, for the present material and conditions, in contrast to other reports in the literature,^{21,24,28} an enhancement of the CO₂ adsorption capacity was not observed due to the presence of moisture. Such differences may be attributed to a higher moisture content and to the dynamic adsorption method used in other studies which cannot guarantee that the material is in equilibrium with the CO₂ content in the gas phase.

A different situation was observed for the sample functionalised with tertiary amine (DEAPTES@SBA-15). The adsorption of CO₂ on the sample with 0.140 mmol g⁻¹ of pre-adsorbed water (this amount is close to the one pre-adsorbed on the sample with primary amine) was significantly enhanced compared with the adsorption on the dry sample (Fig. 1, bottom). The amounts of adsorbed CO₂ were increased by about 0.24 mmol g⁻¹ at low pressures and this difference was maintained in all pressure ranges between the dry sample and the sample with 0.140 mmol g⁻¹ of water. It must be noticed that the amount of CO₂ adsorbed at the surface approaches a ratio of one CO₂ molecule for two amines, in the low-pressure region (below 21 kPa), when water is present in the system (0.140 mmol g⁻¹). An experiment with significantly less amount of pre-adsorbed water (0.045 mmol g⁻¹) was also performed and the effect on the CO₂ adsorption was still quite significant, since an increase of about 0.17 mmol g⁻¹ of CO₂ was observed in all pressure values compared with the dry sample (Fig. 1, bottom).

The results in Fig. 1 for the adsorption of CO₂ on both samples with primary and tertiary amines clearly show that the water causes a significant change in the mechanism of adsorption of CO₂ on surfaces with tertiary amine which leads to increased amounts of adsorbed CO₂. This effect is observed at very low pressures for the tertiary amine (*i.e.*, water increases the affinity of the CO₂ for the surface) but is absent in the case of the primary amine. In fact, no noticeable CO₂ adsorption change was observed for the primary amine in the presence of small amounts of water.

3.3. Experimental strategy to study the effect of moisture on CO₂ speciation

To perform NMR characterization study, all the samples were packed into the NMR sample holder in a controlled atmosphere (see the experimental section for further details). It was found that such rigorous sample handling is of utmost importance as it enables the observation of ¹³C resonances associated with certain CO₂ species that are otherwise not detected.^{4,20}

Tertiary amines are not expected to react directly with CO₂ as they cannot be deprotonated and are bulkier than primary or secondary amines.^{61–63} Instead, tertiary amines capture CO₂ in the aqueous phase through a different mechanism (*via*

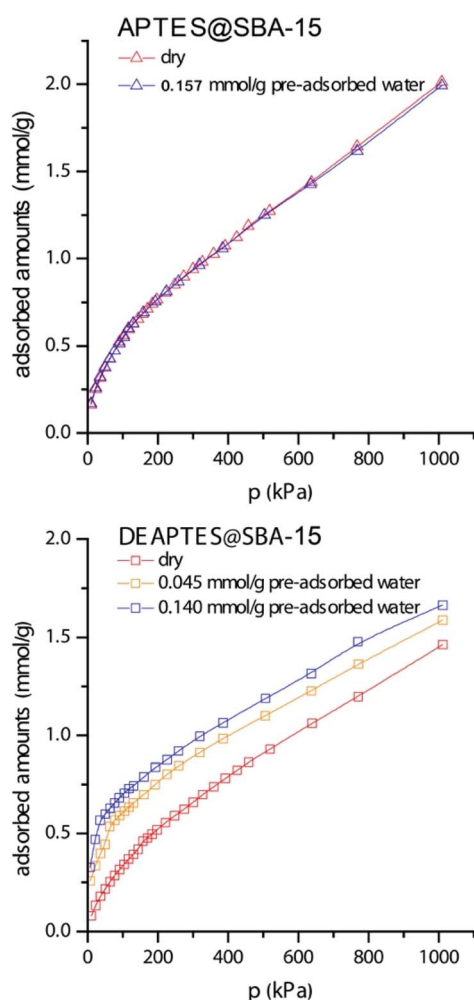


Fig. 1 Adsorption isotherms of CO₂ at 25 °C in dry and wet materials. Results for SBA-15 grafted with primary and tertiary amines at the top and bottom, respectively.



bicarbonate formation), first reported by Donaldson³¹ and later reviewed by Kenig.⁶² First, in water, the tertiary amine dissociates H_2O to form a quaternary cationic species and OH^- . Hydroxide ion then attacks CO_2 to form the bicarbonate anion, which may also form with primary and secondary amines although the rate constants for this base catalysed bicarbonate formation in water are typically smaller than those of the zwitterion mechanism described above.^{31,62} While this mechanism has been mostly studied in the solution state, not much is known about it at the surface of porous materials. One of the goals of this work is to obtain a better molecular-level understanding of the formation of such species on solid surfaces functionalized with amines. For that reason, an experimental protocol was optimised in which primary and tertiary amines are grafted onto SBA-15 and exposed to pure CO_2 (for comparison) and binary $^{13}\text{CO}_2/\text{water}$ mixtures, with different compositions. One sample of APTES@SBA-15 was prepared by loading the material with 2.7 kPa of water vapor followed by adsorption of 100 kPa of $^{13}\text{CO}_2$. For the case of tertiary amines, several

experiments were conducted, in which DEAPTES@SBA-15 was loaded with a specific water vapor partial pressure (0.7, 1.3, and 2.7 kPa) prior to $^{13}\text{CO}_2$ adsorption (2.7, 13, 100–103 kPa).

The experimental strategy designed in this work is significantly different from that of other reported studies where ^{13}C NMR signals for either physisorbed or chemisorbed CO_2 were not detected when the solid sorbent (SBA15 functionalised with *N,N*-dimethyl-3-aminopropyltrimethoxysilane) is mixed with water, forming a slurry.⁴⁰ In contrast, exposure of our amine-functionalized sorbents (dried under high vacuum at 150 °C for 3 h) to a water/ $^{13}\text{CO}_2$ mixture in the gas phase enabled the observation of moisture-induced CO_2 species even for small water partial pressures (*e.g.*, 0.7 kPa). Therefore, we avoided the use of liquid water slurries, which may induce the formation of CO_2 species dissolved in the excess of water, particularly due to the high pH produced by the presence of amines.

The discussion regarding CO_2 speciation in the presence of moisture has been categorized by amine type, primary (Section 3.4) and tertiary (Section 3.5), in an attempt to rationalize the

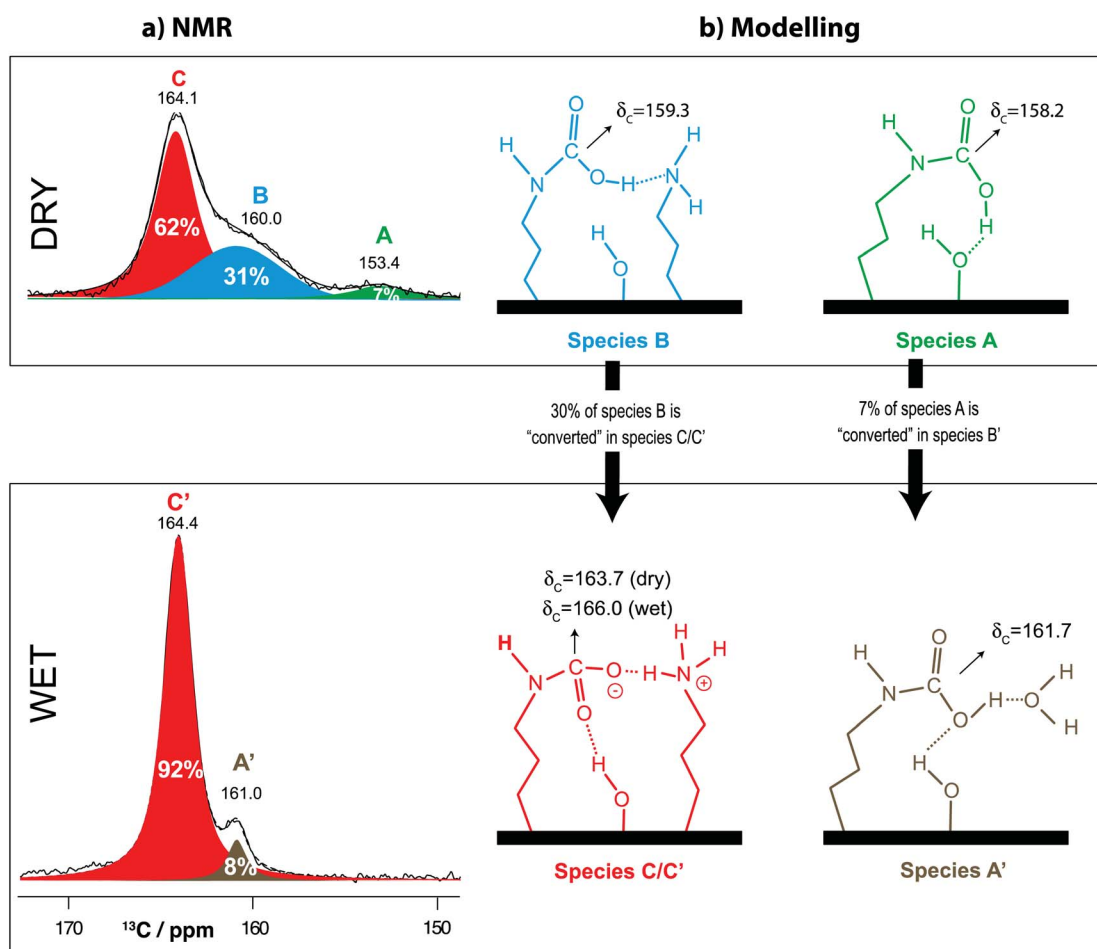


Fig. 2 (a) ^{13}C single-pulse NMR spectra recorded at 12 kHz MAS on a 16.4 T spectrometer of samples containing APTES@SBA-15 loaded with 103 kPa of $^{13}\text{CO}_2$ (top, solid line) and 2.7 kPa of water followed by 100 kPa of $^{13}\text{CO}_2$ (bottom, solid line). Deconvolution of each spectrum is given in the figure (overall fit as a dashed line). Species B was fitted with a Lorentzian function whereas A' had to be fitted using a purely Gaussian function to minimize errors; (b) A, B, and C denote the three resonances attributed to the chemisorbed CO_2 species, according to our previous work.^{4,9,20} Spectra were normalised with respect to their methylene ^{13}C peak areas thus enabling direct comparison of their peak areas. Note that all spectra were recorded using the exact same acquisition and processing parameters and refer to the same batch sample.



observed significant differences in CO₂ speciation as confirmed by their ¹H/¹³C NMR spectra. The role of water in enhancing CO₂ sorption capacity on primary amines due to the formation of bicarbonate species has been suggested based on the hypothesis that the CO₂/amine ratio increases with moisture, but molecular-level insight into this mechanism remains elusive and a rather complex issue, as will be discussed in Section 3.4. The following sections aim at shedding light into this matter.

3.4. Water influence on CO₂ speciation for sorbents modified with primary amines

The ¹³C NMR spectra show that, in the presence of water, the resonance associated with alkylammonium carbamate species (denoted as species C in Fig. 2a) is the most abundant and also the most stable (see Table 1). Under strictly dry conditions, species A, B and C (Fig. 2b) are present in the NMR spectrum of CO₂-loaded SBA15-APTES (Fig. 2a). Henceforth, a prime symbol (') following the letter label (e.g., A', B', C') will be used to denote ¹³C resonances in the NMR spectra of "wet" samples to avoid confusion. Upon water uptake (2.7 kPa of H₂O), the ¹³C NMR spectrum changes considerably; species A (detected in dry samples) disappears, as expected from our previous studies,⁴ and another resonance emerges in moist samples, here denoted as resonance A' (160.9 ppm), which is considerably narrower than resonance B (160.4 ppm) only observed in dry SBA15-APTES (cf. Fig. 2a top and bottom). A' is also slightly shifted by ~0.5 ppm with respect to resonance B. Therefore, NMR data seem to provide strong indications that B and A' are not the same species.

The observed chemical shift changes in ¹³C NMR spectra under dry and moist APTES@SBA-15 (cf. Fig. 2a) provide an excellent opportunity to study the effect of water on CO₂ speciation. A quantitative analysis of the ¹³C NMR spectra reveals that about 31% of carbamic acid species (B), observed under dry conditions, vanishes. The resonance associated with this species (B) seems to have been converted into alkylammonium carbamate ion pairs (C'), in the presence of moisture (62% of C + 31% of B are converted into 92% of C', Fig. 2a). This

observation clearly demonstrates that CO₂ adsorption under humid conditions favours the formation of alkylammonium carbamate ion pairs (C) instead of bicarbonate species as suggested in the literature.^{28,39} This finding complies with previous studies claiming that the amount of carbamic acid (B) is significantly reduced for CO₂ adsorption in a moist environment as compared to dry conditions. Bacsik *et al.*²⁸ suggest that this difference might be due to water mediated formation of ammonium carbamates from carbamic acids being H-bonded with -NH₂ groups (as in the case of species B, Fig. 2b). Molecular modeling results reflect this phenomenon extremely well showing that water induces the proton transfer from carbamic acid to neighbouring amines, reflecting a water-induced transformation of carbamic acid (B) into ammonium carbamate (C') (Fig. 2b). Our molecular modeling study shows that only when the water molecule interacts with isolated carbamic acid species (A) it is possible to stabilize the carbamic acid species labeled A' (Fig. 2b). The final relative stability of the different species (represented in Table 1) shows that ammonium carbamate is substantially more stable than carbamic acid (or bicarbonate) in the presence of water (unlike under dry conditions), supporting the idea that carbamic acid (B) might be converted into ammonium carbamate (C') upon water uptake.

Our previous work showed how sensitive resonance A is to very low H₂O partial pressures. *i.e.*, this resonance (~155 ppm) vanishes as soon as water interacts with the CO₂ binding site.⁴ One may question if water induces desorption of A or if this species is converted to another CO₂ species. Simulation results (shown in Tables 1 and S2†) seem to indicate that adsorbed H₂O and CO₂ are always less stable than the formation of chemisorbed CO₂ species, thus strongly hinting at the latter hypothesis. Due to their similar peak areas, the initial 7% of species A present in the dry APTES@SBA-15 sample (Fig. 2a, top) seems to be converted into species A' (8%, Fig. 2a, bottom), which might be assigned either to putative bicarbonate (presenting the same 1 : 1 CO₂/N stoichiometry as species A, Fig. 2b) or carbamic acid. If we consider that species A' is ascribed to bicarbonate, the amount observed (8%) would not justify what some authors report as an increase in CO₂ uptake under moist conditions.^{1,28,34,35,64} That was not confirmed in our material under the conditions of pressure and temperature of adsorption (Fig. 1). Table 1 presents a comparison of the calculated Gibbs energies of the different species, which may exist when two amines closely interact with each other, under dry and humid conditions. Under dry conditions, the Gibbs energy values for carbamic acid and carbamate species are very similar, with the latter being only 4 kJ mol⁻¹ less stable than the former. When water is introduced into the theoretical system, there is a radical shift in relative stabilities; alkylammonium carbamate stability increases by 29 kJ mol⁻¹ compared to carbamic acid. This supports the idea that the experimentally observed shift from species B to species C is likely due to the conversion of carbamic acid into ammonium carbamate. It seems that the intricate network of hydrogen bonded water molecules aids in the proton transfer from the carbamate group to the amino group. Moreover, under humid conditions, the bicarbonate species is even less stable than carbamic acid (45 kJ mol⁻¹ less stable than

Table 1 Calculated Gibbs energy differences of CO₂ species formed, for a cluster containing two amines and one silanol, under dry and humid conditions

Species	ΔG (kJ mol ⁻¹)
Without H₂O	
Adsorbed CO ₂	43
Ammonium carbamate	4
Carbamic acid	0
With H₂O	
Adsorbed CO ₂ and H ₂ O	68
Bicarbonate/carbonic acid	45
Carbamic acid	29
Ammonium carbamate	0



ammonium carbamate, Table 1), which does not vouch for a dominant presence of bicarbonate species.

Successive experimental and theoretical results^{3,4,9,20,38,43,44,65} indicate that both carbamic acid and bicarbonate resonate at 159–162 ppm, thus making it particularly difficult to distinguish between these two species on the basis of NMR spectra alone. Considering the computational results and the ¹³C NMR quantitative analysis shown previously, we assign the CO₂ species A' to a non-paired (isolated) carbamic acid species interacting with water molecules (with or without neighbouring silanols), the same that generates resonance A under dry conditions (Fig. 2). Indeed, the addition of water molecules into the simulation clusters systematically shifts the ¹³C resonances attributed to carbamic acid, towards higher CS values (Table S3†), *i.e.*, in the direction A → A'.

With the strategy described in this work, it was possible to evaluate the influence of water in the CO₂ chemisorption process on primary amines. To unequivocally identify the formation of bicarbonate species, a complementary study using tertiary amine-grafted materials is also pursued in Section 3.5 as carbamic acid formation is not favoured by bulkier amines, thus providing additional structural insight. Moreover, studies on CO₂ speciation involving silica materials modified with tertiary amines under rigorous control over partial pressures of adsorbed gases were not reported so far.

3.5. Water influence on CO₂ speciation for sorbents modified with tertiary amines

3.5.1. Detecting amine–silanol interactions prior to CO₂ adsorption. The participation of silanol protons in intermolecular interactions involving alkylamine and/or carbamic acid/carbamate species is not straightforward to study because amine-grafted mesoporous silicas contain a significant amount of hydrogen containing functional groups giving rise to ¹H signals often overlapped in the NMR spectra. Fig. 3 shows multiple ¹H MAS NMR spectra in dry and wet SBA-15 with and without amine functionalization to mitigate some of the above-mentioned problems associated with ¹H NMR spectroscopy, thus rendering the technique more insightful. The 1D ¹H NMR spectra of tertiary amine-grafted SBA-15 (DEAPTES@SBA-15) exhibit resonances at 0.9, 1.3, 2.4 and 3.4 ppm assigned to the different CH₂/CH₃ protons from the grafted amine moiety. The resonance at *ca.* 7.2 ppm is present in the ¹H NMR spectra of samples not exposed to water and CO₂, suggesting that this resonance might be attributed to hydrogen atoms from silanol groups interacting with neighbouring amines. It is worth mentioning that the parent sample (SBA-15) depicts a strong Si–OH proton peak at *ca.* 1.6 ppm, which disappears upon DEAPTES functionalization with the simultaneous appearance of a faint resonance observed at *ca.* 7.2 ppm. This observation strongly suggests that the few silanol groups still present after amine functionalization of the silica surface are all engaged in strong H-bonds with amines. Interestingly, the calculated ¹H CSs of a structure model with DEAPTES forming a hydrogen bond with silanol protons also give rise to a resonance in

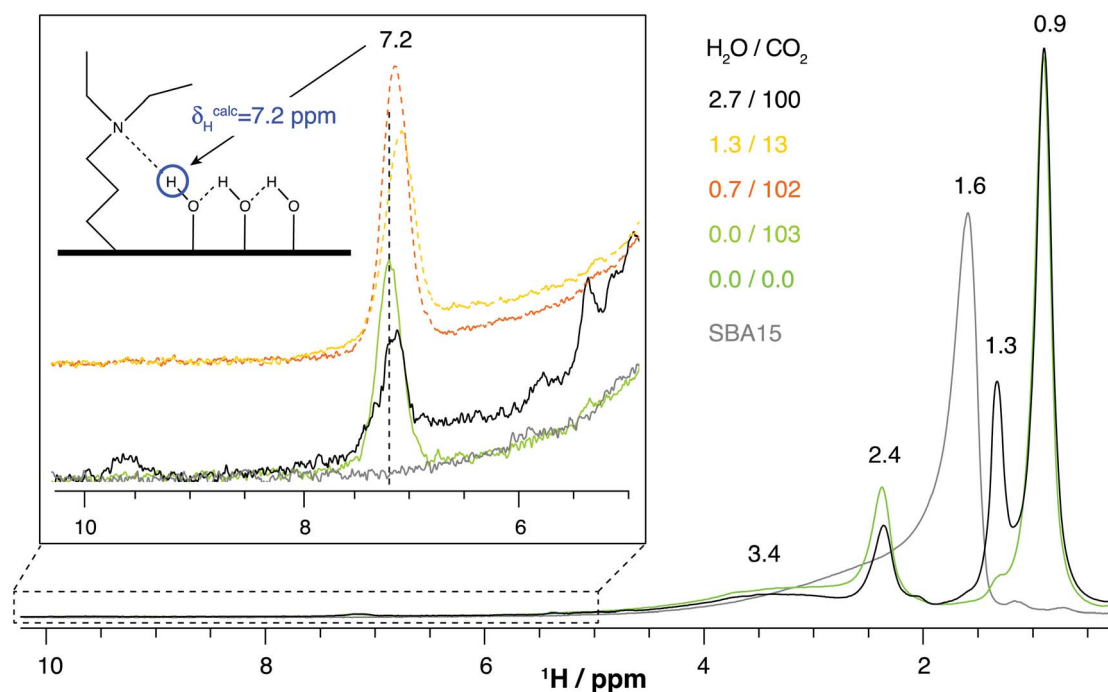


Fig. 3 ¹H Hahn-echo NMR spectra of pristine SBA-15, DEAPTES@SBA-15 and the latter exposed to distinct combinations of water and CO₂ partial pressures (in kPa), recorded at 16.4 T with a spinning rate of 15 kHz. Additional parameters are provided in the experimental section. The structure model exhibiting the ¹H resonance at 7.2 ppm is shown in Fig. S6.†



a similar ^1H CS as shown in Fig. S6.† However, a resonance slightly shifted to lower ^1H CS (*ca.* 7.1 ppm) is also observed in the same region for samples in which CO_2 has been adsorbed under wet conditions. The presence of this resonance is also compatible with the bicarbonate OH proton as supported by ^1H CS DFT calculations (Fig. 5). Thus, both ^1H resonances are likely to be overlapped.

3.5.2. Understanding the formation mechanism of moisture-induced CO_2 species. Different combinations of $\text{H}_2\text{O}/\text{CO}_2$ partial pressures were tested for DEAPTES@SBA-15, as described in Section 3.3. These combinations were monitored by recording ^{13}C CPMAS NMR spectra (Fig. 4), depicting a dominant resonance centred at *ca.* 161 ppm, assigned to the bicarbonate species (Fig. 4 and 5). We demonstrate that bicarbonate species are detected in DEAPTES@SBA-15 adsorbents exposed even at water vapor pressures as low as 0.7 kPa, which has not hitherto been reported in the literature, to the best of our knowledge. Other studies were only able to detect bicarbonate species in slurries of the materials in liquid water.^{40,43}

For comparison purposes, an additional sample was prepared, in which pure $^{13}\text{CO}_2$ was adsorbed under dry conditions (103 kPa of $^{13}\text{CO}_2$). In this case, a weak resonance appears at 154.8 ppm (Fig. 4), ascribed to carbamic acid-like species as supported by the structure models presented in Fig. 6a and c. The two models depicted in Fig. 6a–d exhibit combinations of possible structures resulting from the reaction between 3^{ary} amines and CO_2 . These models are all compatible with CO_2 -

adducts giving rise to a ^{13}C chemical shift lower than 156 ppm, supporting the fact that the activation of CO_2 by 3^{ary} amines is possible under dry conditions albeit to a very small extent given the low intensity of the resonance. Notice that a hypothetical CO_2 zwitterion (Fig. 6b and d) was also computed to check whether such species could be compatible with our experimental ^{13}C CS (154.8 ppm). A calculated ^{13}C CS of 141.6 ppm was obtained for the zwitterion, clearly far from this resonance observed at 154.8 ppm, presumably associated with carbamic acid species (Fig. 6a and c) generated by proton transfer from surrounding silanol groups to the N-COO- group. Such silanol groups are likely to possess stronger Brønsted acidity, induced by framework defects, thus facilitating the proton extraction by $^-\text{N}-\text{COO}^-$ zwitterion species. Thus, the number of amines that can bind CO_2 under dry conditions is limited to those that have Brønsted acid groups in the vicinity, explaining in this way the lower intensity of the 154.8 ppm peak (Fig. 4).

The presence of this ^{13}C resonance at 154.8 ppm is typical of chemisorbed CO_2 -adducts of the type A (carbamic acid), as found in 1^{ary} amines (Fig. 2). This may seem counterintuitive for 3^{ary} amines as their bulkiness and the absence of NH protons are believed to hinder the formation of carbamic acid species. Hence, the presence of this resonance in the ^{13}C MAS NMR spectrum strongly supports the fact that 3^{ary} amines can act as a nucleophilic agent and react with the CO_2 Lewis acid. Molecular models containing 3^{ary} amines bonded to CO_2 , also support this fact as the resulting carbonyl carbon exhibits

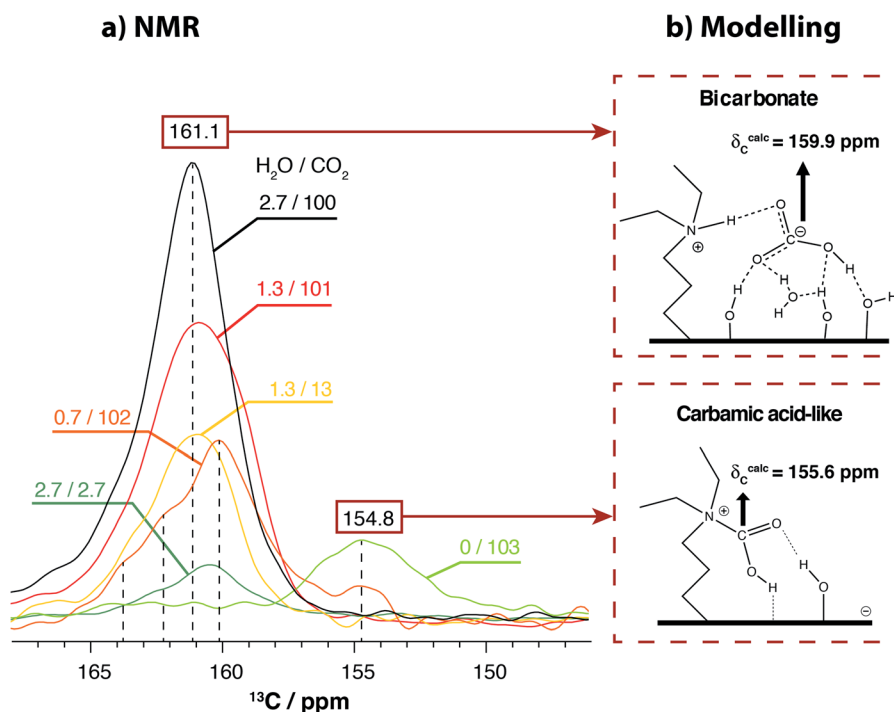


Fig. 4 (a) ^{13}C CPMAS NMR spectra of DEAPTES@SBA-15 materials, recorded at 16.4 T with a spinning rate of 12 kHz, after exposure to a given partial pressure of H_2O followed by exposure to $^{13}\text{CO}_2$. Specific partial pressures are given in the figure, in kPa. (b) Two-dimensional representation of the optimised structures for bicarbonate and carbamic acid-like species (the corresponding 3D structure models are depicted in Fig. 5 and 6). Spectra were normalised with respect to the intensity of the propylamine carbons to obtain a fair comparison between NMR spectra at varying CO_2 and H_2O partial pressures.



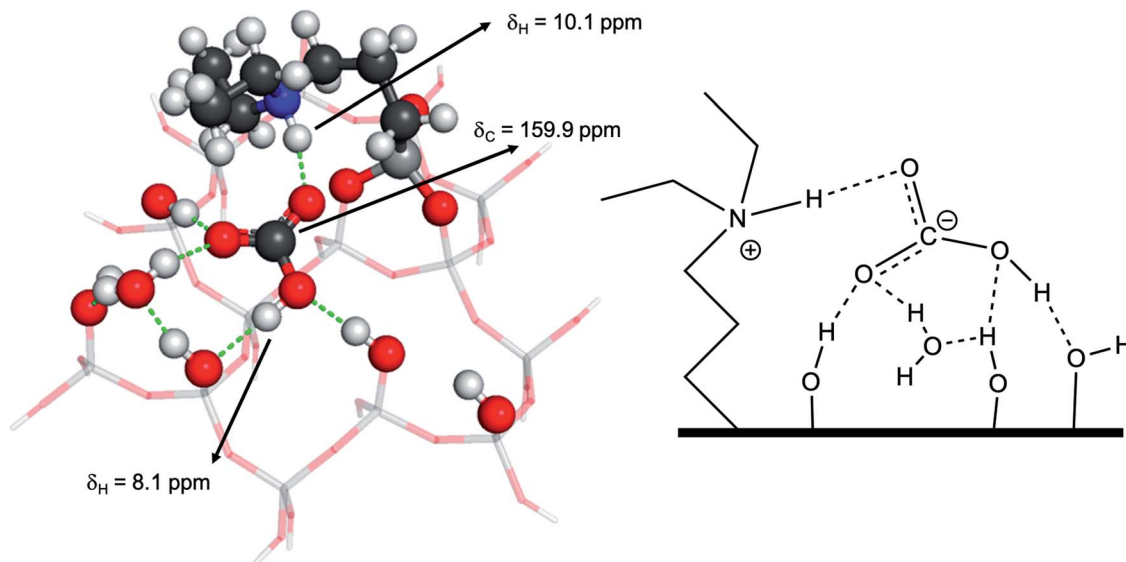


Fig. 5 Structure model representations of a bicarbonate ion interacting with a tertiary ammonium ion, surrounded by hydroxyl groups and a water molecule. The 3D-dimensional representation corresponds to the optimised structure with chemical shifts closest to those observed experimentally. The theoretical chemical shifts associated with different atoms in the structure are also indicated.

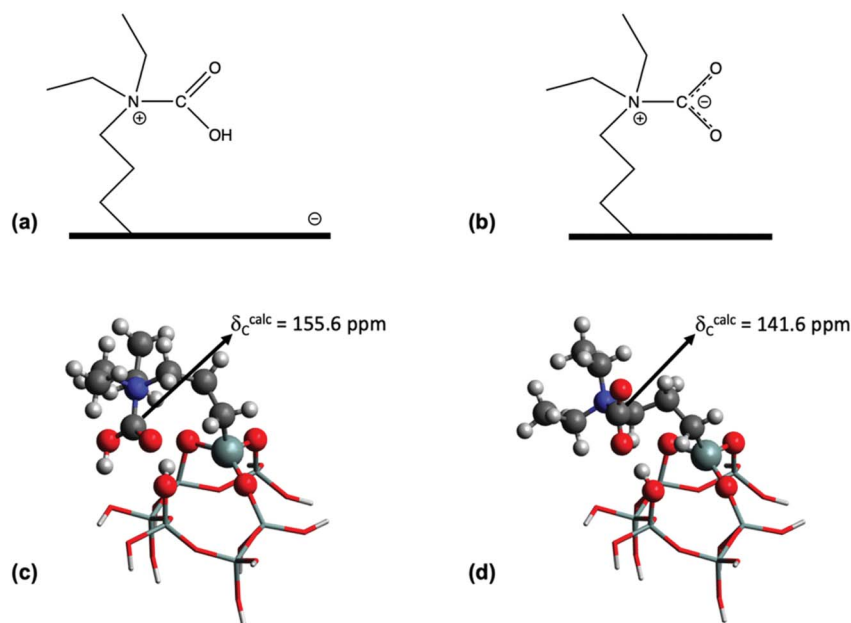


Fig. 6 Two- (a and b) and three-dimensional (c and d) representations of the species formed by the chemisorption of CO_2 onto tertiary amines in the absence of water. (a) and (c) Carbamic acid-like species (the surface negative charge depicts deprotonated silanol groups, see the text for further details); (b) and (d) zwitterionic carbamate-like species. The three-dimensional representation corresponds to the optimised structure with the lowest energy among the many performed. The chemical shifts associated with the carbon are indicated in the three-dimensional representation.

a theoretical ^{13}C CS of 155.6 ppm (Fig. 6), typical of carbamic acid functional groups. Note that this resonance vanishes by just exposing the sample at very low water vapor pressure (0.7 kPa), resembling the behaviour of CO_2 species A in primary amines as reported in our previous work.^{4,9,20} We emphasize that the disappearance of this resonance depends on the order

in which CO_2 and H_2O are adsorbed and in their relative partial pressures (Fig. 7). Notice that only when a significant difference between the partial pressures of both gases is used, the resulting ^{13}C NMR spectrum is altered depending on whether water is added first or if both gases are added simultaneously (Fig. 7). For example, the sample loaded with 1.3 kPa of water vapor and



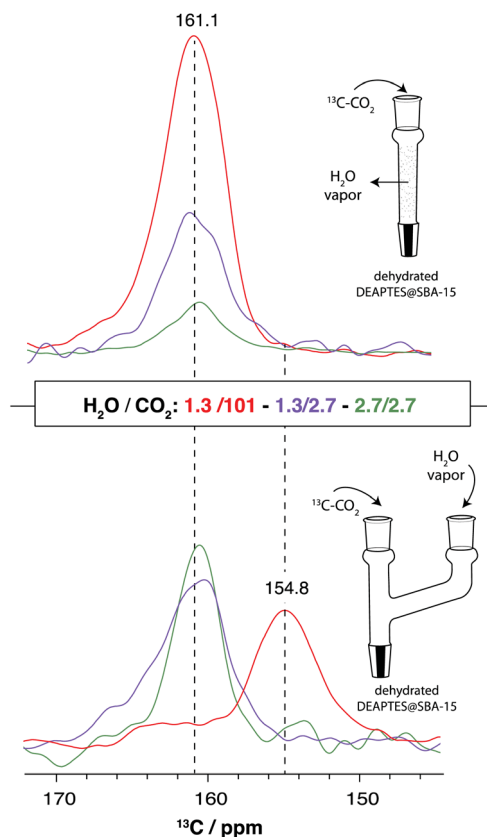


Fig. 7 ^{13}C CPMAS NMR spectra of DEAPTES@SBA-15 materials, recorded at 16.4 T with a spinning rate of 12 kHz, after exposure to a given partial pressure (in kPa) of H_2O followed by exposure to $^{13}\text{CO}_2$ (top) and simultaneously exposed to H_2O and $^{13}\text{CO}_2$ (bottom).

101 kPa of $^{13}\text{CO}_2$ gives rise to a single ^{13}C resonance at 161 ppm, when the material is exposed to water vapour prior to CO_2 adsorption. On the other hand, on exposing the material simultaneously to a binary mixture containing both water vapor and $^{13}\text{CO}_2$ at similar partial pressures, a peak emerges at 154.8 ppm (Fig. 7, bottom), resembling the spectrum of pure CO_2 loaded materials. Although, in both cases described earlier, the water vapor pressure is kept constant (1.3 kPa), the order in which water is mixed with CO_2 will favour the formation of either carbamic acid or bicarbonate species (Fig. 7 and 4b). The formation of the former species (under moist conditions) can be explained by the much lower accessibility of water to the amine binding sites when CO_2 concentration is overwhelmingly superior to that of water when both gases are adsorbed simultaneously.

Focusing on samples with a similar amount of CO_2 partial pressure (ca. 100 kPa), namely samples with the following $\text{H}_2\text{O}/\text{CO}_2$ content: 2.7/100, 1.3/101 and 0.7/102 (black, red and orange lines in Fig. 4a, respectively; units in kPa), it is possible to observe that as the partial pressure of water vapor increases, the intensity of the peak also increases and the centre of the main peak shifts (from 160.1 ppm) towards higher chemical shift values, up to the final value of 161.1 ppm. The same observation is valid for the sample with the same partial pressure of CO_2 and

H_2O (2.7/2.7, dark green line in Fig. 4a), in which the peak centre is slightly shifted to lower chemical shift values (ca. 160.5 ppm). In this case, although the amount of water is the same as for sample 2.7/100 (black line, Fig. 4a), the amount of CO_2 available (2.7 kPa) is not sufficient to generate as much bicarbonate (centred at 161.1 ppm) as in the 2.7/100 sample. It is worth mentioning that 2.7 kPa is the highest water vapor pressure we were able to admit, at room temperature. For the sample loaded with 0.7 kPa of water vapor (orange line in Fig. 4a), the spectrum is more complex, showing at least three distinct chemical environments in the region between 161 and 164 ppm, associated with the formation of moisture-induced CO_2 species (see dashed lines in Fig. 4a).

To obtain a deeper insight into the intermolecular interactions associated with the formation of bicarbonate species, computer models comprising this species engaged in multiple H-bonding modes were investigated. Fig. 5 depicts the lowest-energy optimised structure model for the bicarbonate ion interacting with a tertiary ammonium ion, surrounded by silanol groups and a water molecule with the corresponding calculated and experimental ^1H and ^{13}C CS. This model was the most compatible with the NMR data; i.e., calculated ^{13}C and ^1H CS values obtained from this model (159.9 and 8.1 ppm, respectively) are in close agreement with the experimental CS (cf. Fig. 4 and 5).

To better support the proposed model for the bicarbonate species (presented in Fig. 5), we have explored ^1H NMR-based techniques, namely two-dimensional (2D) ^1H - ^{13}C (Fig. 8) and ^1H - ^{29}Si (Fig. S7†) HETCOR NMR experiments that rely on through-space dipole-dipole interactions to selectively detect $^1\text{H}\cdots^{13}\text{C}$ and $^1\text{H}\cdots^{29}\text{Si}$ nuclear proximities, respectively. The 2D ^1H - ^{13}C HETCOR spectrum (Fig. 8) of DEAPTES@SBA-15, after exposure to 2.7 kPa of water and 100 kPa $^{13}\text{CO}_2$, shows ^1H - ^{13}C cross-peaks arising from the alkylamine carbons (resonating at 9.9, 20.2, 46.6 and 55.7 ppm) interacting with the different methylene (CH_2) and methyl (CH_3) protons (between 0 and 5 ppm) from the amine moiety (see assignment in Fig. 8).

The bicarbonate ^{13}C resonance at 161.1 ppm presents two strong correlations with ^1H resonances at 1.0 and 3.2 ppm. The former is assigned to both $\text{Si}-\text{CH}_2$ and CH_3 groups, whose signals overlap, while the latter is associated with two ^{13}C resonances: the methylene carbon adjacent to the methyl group at 46.6 ppm (marked grey in Fig. 8) and the bicarbonate carbon. This seems to suggest that the CH_2 protons at 3.2 ppm are in close proximity to the bicarbonate molecule as demonstrated in the model shown in Fig. 5.

Even though the low signal-to-noise ratio presented in this spectrum, in the ^1H CS region between 6 and 10 ppm (Fig. 8, 4 days acquisition time), does not allow us to distinguish among the different ^1H environments interacting with the bicarbonate molecule ($\delta_{\text{C}} = 161.1$ ppm, Fig. 5), a ^{13}C - ^1H cross-peak is clearly visible in that region centered at ca. 7–8 ppm. Calculated ^1H and ^{13}C CSs (shown in Fig. 8, close to the respective atoms) from the proposed lowest-energy DEAPTES-bicarbonate structure model (Fig. 5) exhibit protons that are strongly deshielded compared to the calculated ^1H CS for isolated DEAPTES (Fig. S8†) due to the polarization effect of bicarbonate molecules in their



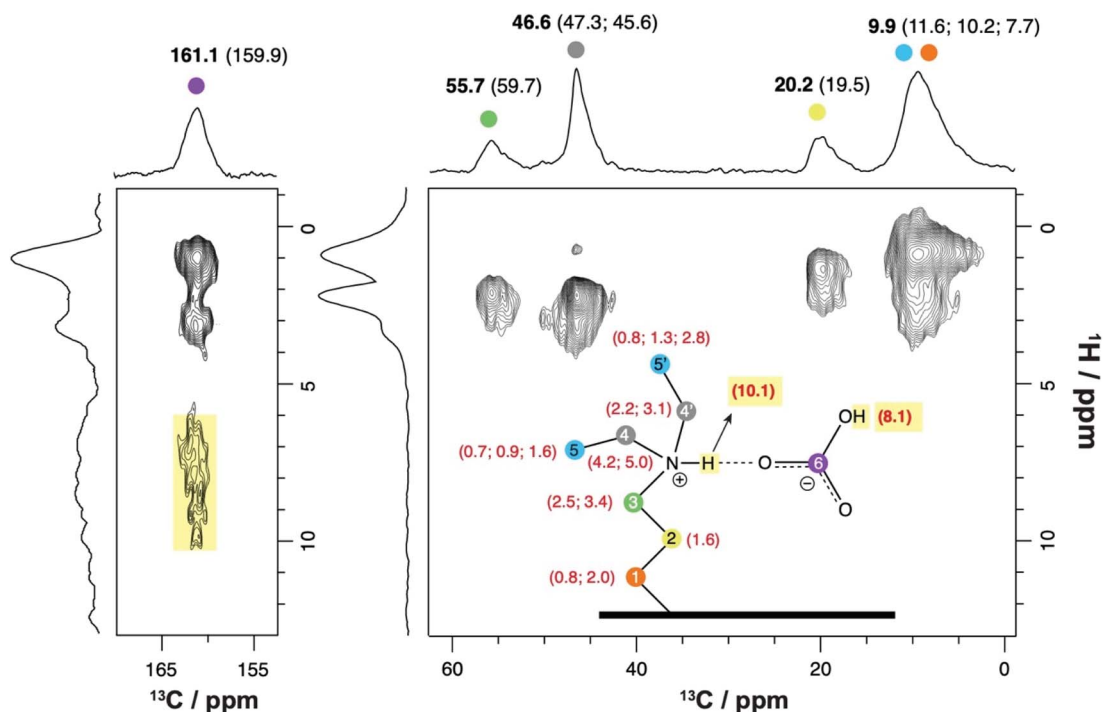


Fig. 8 ^1H - ^{13}C CPMAS HETCOR NMR spectrum of DEAPTES@SBA-15 loaded with 2.7 kPa of water and 100 kPa of $^{13}\text{CO}_2$, recorded at 16.4 T with a spinning rate of 12 kHz and using a contact time of 2 ms. Additional parameters are provided in the experimental section. Numbers in black and bold depict experimental ^{13}C CSs (in ppm) and numbers in parenthesis (red for ^1H , black for ^{13}C) refer to calculated CSs from the structure model displayed in Fig. 5. The calculated ^1H CSs for N-H and bicarbonate protons are highlighted in yellow.

proximity. The DEAPTES-bicarbonate structure model shows that specific ^1H CSs are deshielded with respect to isolated DEAPTES *i.e.*, ^1H CSs from C(1) H_2 and C(5') H_3 protons are shifted from 0.8 to 2.0 and from 1.6 to 2.8 ppm, respectively, due to their interaction with the bicarbonate oxygen atom through $\text{CH}\cdots\text{O}$ weak H-bonds (Fig. 5). The 2D ^1H - ^{13}C HETCOR spectrum of DEAPTES@SBA-15 seems to agree with this observation as both these functional groups contribute to the cross-peaks appearing at $\delta(^1\text{H}) \geq 2$ ppm. The calculated ^1H CS of the DEAPTES ^+NH group appears at 10.1 ppm upon H-bonding with bicarbonate, which is difficult to ascertain through comparison with the experimental data. Nevertheless, in addition to the peak at *ca.* 7.1 ppm, observed in the ^1H NMR spectra (Fig. 3), a weak resonance at 9.6 ppm is also visible. Although this peak (9.6 ppm, Fig. 3) matches appreciably well with the calculated 10.1 ppm for the bicarbonate model (N-H proton), we prefer to remain conservative by not proposing an unequivocal assignment of this resonance.

The bicarbonate molecular pair model exhibits an OH proton at 8.1 ppm, correlated with the bicarbonate ^{13}C resonance at 159.9 ppm (Fig. 5), which is in good agreement with the experimental NMR data displaying a cross-peak at similar ^1H and ^{13}C CS values, at 7–8 ppm and *ca.* 161 ppm, respectively (Fig. 8).

4. Conclusions

The CO_2 speciation on primary and tertiary amine-modified mesoporous silicas under dry and wet conditions has been

studied combining solid-state NMR and computer modelling. Adsorption of $^{13}\text{CO}_2$ and water vapor under controlled partial pressures, followed by the application of solid-state NMR methods was essential to gather molecular-level information on the moisture-induced CO_2 species formed in such sorbent materials.

Our study shows that CO_2 adsorbed to primary amines, under humid conditions favours the formation of alkylammonium carbamate ion pairs instead of bicarbonate species. Molecular modeling and theoretical Gibbs energy results agree with a water-induced transformation of carbamic acid into alkylammonium carbamate, supported by the fact that the latter species is energetically much more stable than carbamic acid (or bicarbonate) in the presence of water, as opposed to dry conditions. Adsorption data of APTES@SBA-15 with pure CO_2 and mixed $\text{CO}_2 + \text{H}_2\text{O}$ show that water does not seem to increase the CO_2 adsorption up to ~ 1000 kPa.

In contrast, for the case of tertiary amines, the CO_2 adsorbed amounts were significantly enhanced with the presence of minor amounts of water at the surface (0.140 mmol g^{-1} of water leads to a 0.24 mmol g^{-1} increase in adsorbed CO_2). Special focus was given to two chemisorbed CO_2 species identified, by NMR and DFT calculations, from distinct carbonyl environments resonating at $\delta_{\text{C}} \sim 161$ and 155 ppm, assigned to bicarbonate and a carbamic acid-like species, respectively. Unlike previous studies in the literature, that detect the formation of bicarbonate species only when slurries are formed, in this study bicarbonate is detected for DEAPTES@SBA-15 exposed to water



vapor pressures from 0.7 kPa up to values close to water vapor saturation pressure at ambient temperature (2.7 kPa).

The presence of a ^{13}C resonance at ~ 155 ppm and the agreement with the calculated ^{13}C CS extracted from structure models (<156 ppm) support the fact that tertiary amines may directly activate CO_2 to form carbamic acid-like species in the vicinity of Brönsted protons covering the silica surface. This species was observed under dry conditions, as well as under the adsorption of a $\text{CO}_2/\text{H}_2\text{O}$ binary mixture with partial pressures of 101 and 1.3 kPa, respectively. Atomic scale studies of CO_2 speciation upon gas adsorption in solid surfaces are still scarce; this work attempts to shorten this gap by shedding light on how the chemisorbed CO_2 species are formed and interconverted, under moist conditions, using amine residues presenting distinct bulkiness.

Conflicts of interest

There are no conflicts to declare.

Acknowledgements

This work was developed in the scope of project CICECO-Aveiro Institute of Materials from the University of Aveiro ref. UIDB/50011/2020 & UIDP/50011/2020, project CERENA ref. UIDB/04028/2020 & UIDP/04028/2020. We also acknowledge funding from projects ref. PTDC/QUI-QFI/28747/2017 (GAS2MAT-DNPSENS - POCI-01-0145-FEDER-028747), PTDC/QUI-QFI/31002/2017 (SILVIA - CENTRO-01-0145-FEDER-31002), PTDC/QEQ-QAN/6373/2014 and Smart Green Homes POCI-01-0247-FEDER-007678, a co-promotion between Bosch Termotecnologia S.A. and the University of Aveiro. These projects are financed through FCT/MEC and co-financed by FEDER under the PT2020 Partnership Agreement. The NMR spectrometers are part of the National NMR Network (PTNMR) and are partially supported by Infrastructure Project 022161 (co-financed by FEDER through COMPETE 2020, POCI and PORL and FCT through PIDDAC). This work has received funding from the European Research Council (ERC) under the European Union's Horizon 2020 research and innovation programme (grant agreement no. 865974).

References

- 1 E. S. Sanz-Pérez, C. R. Murdock, S. A. Didas and C. W. Jones, *Chem. Rev.*, 2016, **116**, 11840–11876.
- 2 P. M. MacQueen, R. A. Bach, C. T. P. MacLean and S. L. MacQuarrie, *J. Phys. Chem. C*, 2014, **118**, 5239–5242.
- 3 M. L. Pinto, L. L. Mafrá, J. M. Guil, J. Pires and J. Rocha, *Chem. Mater.*, 2011, **23**, 1387–1395.
- 4 L. Mafrá, T. Čendak, S. Schneider, P. V. Wiper, J. Pires, J. R. B. Gomes and M. L. Pinto, *J. Am. Chem. Soc.*, 2017, **139**, 389–408.
- 5 D. Reichle, J. Houghton, S. Benson, J. Clarke, R. Dahlman, D. G. Hendrey, H. Herzog, J. Hunter-Cevera, G. Jacobs, R. Judkins, B. Kane, J. Ekmann, J. Ogden, A. Palmisano, D. R. Socolow, J. Stringer, T. Surles, A. Wolsky, N. Woodward, D. M. York and D. Ii, *Carbon Sequestration – State of the Science*, Washington DC, 1999.
- 6 B. A. Oyenekan and G. T. Rochelle, *AIChE J.*, 2007, **53**, 3144–3154.
- 7 A. S. Bhowan and B. C. Freeman, *Environ. Sci. Technol.*, 2011, **45**, 8624–8632.
- 8 X. Xu, C. Song, B. G. Miller and A. W. Scaroni, *Ind. Eng. Chem. Res.*, 2005, **44**, 8113–8119.
- 9 R. Afonso, M. Sardo, L. Mafrá and J. R. B. Gomes, *Environ. Sci. Technol.*, 2019, **53**, 2758–2767.
- 10 S. Nandi, S. Collins, D. Chakraborty, D. Banerjee, P. K. Thallapally, T. K. Woo and R. Vaidhyanathan, *J. Am. Chem. Soc.*, 2017, **139**, 1734–1737.
- 11 P. Nugent, Y. Belmabkhout, S. D. Burd, A. J. Cairns, R. Luebke, K. Forrest, T. Pham, S. Ma, B. Space, L. Wojtas, M. Eddaoudi and M. J. Zaworotko, *Nature*, 2013, **495**, 80–84.
- 12 A. Asghar, N. Iqbal, L. Aftab, T. Noor, B. M. Kariuki, L. Kidwell and T. L. Easun, *R. Soc. Open Sci.*, 2020, **7**, 191934.
- 13 Y. Chen, Z. Qiao, J. Huang, H. Wu, J. Xiao, Q. Xia, H. Xi, J. Hu, J. Zhou and Z. Li, *ACS Appl. Mater. Interfaces*, 2018, **10**, 38638–38647.
- 14 S. Chand, A. Pal and M. C. Das, *Chem.–Eur. J.*, 2018, **24**, 5982–5986.
- 15 J. Zhu, L. Wu, Z. Bu, S. Jie and B.-G. Li, *ACS Omega*, 2019, **4**, 3188–3197.
- 16 Y. Wang, Z. Hu, T. Kundu, Y. Cheng, J. Dong, Y. Qian, L. Zhai and D. Zhao, *ACS Sustainable Chem. Eng.*, 2018, **6**, 11904–11912.
- 17 D. Andirova, Y. Lei, X. Zhao and S. Choi, *ChemSusChem*, 2015, **8**, 3405–3409.
- 18 I. Yanase, K. Sato, H. Kobayashi, T. Doe and T. Naka, *Chem. Eng. J.*, 2019, **356**, 81–90.
- 19 K. Essaki, K. Nakagawa, M. Kato and H. Uemoto, *J. Chem. Eng.*, 2004, **37**, 772–777.
- 20 T. Čendak, L. Sequeira, M. Sardo, A. Valente, M. L. Pinto and L. Mafrá, *Chem.–Eur. J.*, 2018, **24**, 10136–10145.
- 21 A. Sayari and Y. Belmabkhout, *J. Am. Chem. Soc.*, 2010, **132**, 6312–6314.
- 22 E. E. Ünveren, B. Ö. Monkul, Ş. Sarioğlu, N. Karademir and E. Alper, *Petroleum*, 2017, **3**, 37–50.
- 23 J. Yu and S. S. C. Chuang, *Ind. Eng. Chem. Res.*, 2017, **56**, 6337–6347.
- 24 H. Zhang, A. Goeppert, G. A. Olah and G. K. S. Prakash, *J. CO₂ Util.*, 2017, **19**, 91–99.
- 25 N. Hiyoshi, K. Yogo and T. Yashima, *Microporous Mesoporous Mater.*, 2005, **84**, 357–365.
- 26 N. Hiyoshi, K. Yogo and T. Yashima, *Stud. Surf. Sci. Catal.*, 2004, **153**, 417–422.
- 27 N. Hiyoshi, K. Yogo and T. Yashima, *Chem. Lett.*, 2004, **33**, 510–511.
- 28 Z. Bacsik, N. Ahlsten, A. Ziadi, G. Zhao, A. E. Garcia-Bennett, B. Martín-Matute and N. Hedin, *Langmuir*, 2011, **27**, 11118–11128.
- 29 G. P. Knowles, S. W. Delaney and A. L. Chaffee, *Ind. Eng. Chem. Res.*, 2006, **45**, 2626–2633.
- 30 G. P. Knowles, J. V. Graham, S. W. Delaney and A. L. Chaffee, *Fuel Process. Technol.*, 2005, **86**, 1435–1448.



- 31 T. L. Donaldson and Y. N. Nguyen, *Ind. Eng. Chem. Fundam.*, 1980, **19**, 260–266.
- 32 S. Choi, J. H. Drese and C. W. Jones, *ChemSusChem*, 2009, **2**, 796–854.
- 33 P. Bollini, S. a. Didas and C. W. Jones, *J. Mater. Chem.*, 2011, **21**, 15100–15120.
- 34 M. W. Hahn, M. Steib, A. Jentys and J. A. Lercher, *J. Phys. Chem. C*, 2015, **119**, 4126–4135.
- 35 K. Li, J. D. Kress and D. S. Mebane, *J. Phys. Chem. C*, 2016, **120**, 23683–23691.
- 36 R. Zhang, Z. Liang, H. Liu, W. Rongwong, X. Luo, R. Idem and Q. Yang, *Ind. Eng. Chem. Res.*, 2016, **55**, 3710–3717.
- 37 J. P. Jakobsen, J. Krane and H. F. Svendsen, *Ind. Eng. Chem. Res.*, 2005, **44**, 9894–9903.
- 38 G. S. Foo, J. J. Lee, C.-H. Chen, S. E. Hayes, C. Sievers and C. W. Jones, *ChemSusChem*, 2017, **10**, 266–276.
- 39 S. A. Didas, M. A. Sakwa-novak, G. S. Foo, C. Sievers and C. W. Jones, *J. Phys. Chem. Lett.*, 2014, **5**, 4194–4200.
- 40 C.-H. Chen, D. Shimon, J. J. Lee, F. Mentink-Vigier, I. Hung, C. Sievers, C. W. Jones and S. E. Hayes, *J. Am. Chem. Soc.*, 2018, **140**, 8648–8651.
- 41 K. Gottschling, L. Stegbauer, G. Savasci, N. A. Prisco, Z. J. Berkson, C. Ochsenfeld, B. F. Chmelka and B. V. Lotsch, *Chem. Mater.*, 2019, **31**, 1946–1955.
- 42 J. K. Moore, M. A. Sakwa-Novak, W. Chaikittisilp, A. K. Mehta, M. S. Conradi, C. W. Jones and S. E. Hayes, *Environ. Sci. Technol.*, 2015, **49**, 13684–13691.
- 43 C.-H. Chen, D. Shimon, J. J. Lee, S. A. Didas, A. K. Mehta, C. Sievers, C. W. Jones and S. E. Hayes, *Environ. Sci. Technol.*, 2017, **51**, 6553–6559.
- 44 J. J. Lee, C.-H. Chen, D. Shimon, S. E. Hayes, C. Sievers and C. W. Jones, *J. Phys. Chem. C*, 2017, **121**, 23480–23487.
- 45 X. Li, E. Hagaman, C. Tsouris and J. W. Lee, *Energy Fuels*, 2003, **17**, 69–74.
- 46 L. Mafra, T. Čendak, S. Schneider, P. V. Wiper, J. Pires, J. R. B. Gomes and M. L. Pinto, *Chem. Eng. J.*, 2018, **336**, 612–621.
- 47 S. M. Antao, I. Hassan, J. Wang, P. L. Lee and B. H. Toby, *Can. Mineral.*, 2008, **46**, 1501–1509.
- 48 J. R. B. Gomes, M. N. D. S. Cordeiro and M. Jorge, *Geochim. Cosmochim. Acta*, 2008, **72**, 4421–4439.
- 49 J. R. Gomes, F. Illas and B. Silvi, *Chem. Phys. Lett.*, 2004, **388**, 132–138.
- 50 N. Lopez, F. Illas and G. Pacchioni, *J. Am. Chem. Soc.*, 1999, **121**, 813–821.
- 51 Y. Zhao and D. G. Truhlar, *Theor. Chem. Acc.*, 2007, **120**, 215–241.
- 52 Y. Zhao and D. G. Truhlar, *J. Phys. Chem. A*, 2006, **110**, 5121–5129.
- 53 P. C. Hariharan and J. A. Pople, *Theor. Chim. Acta*, 1973, **28**, 213–222.
- 54 M. M. Francel, W. J. Pietro, W. J. Hehre, J. S. Binkley, M. S. Gordon, D. J. DeFrees and J. A. Pople, *J. Chem. Phys.*, 1982, **77**, 3654–3665.
- 55 M. J. Frisch, G. W. Trucks, H. B. Schlegel, G. E. Scuseria, M. A. Robb, J. R. Cheeseman, G. Scalmani, V. Barone, B. Mennucci, G. A. Petersson, H. Nakatsuji, M. Caricato, X. Li, H. P. Hratchian, A. F. Izmaylov, J. Bloino, G. Zheng, J. L. Sonnenberg, M. Hada, M. Ehara, K. Toyota, R. Fukuda, J. Hasegawa, M. Ishida, T. Nakajima, Y. Honda, O. Kitao, H. Nakai, T. Vreven, J. A. Jr., J. E. Peralta, F. Ogliaro, M. Bearpark, J. J. Heyd, E. Brothers, K. N. Kudin, V. N. Staroverov, T. Keith, R. Kobayashi, J. Normand, K. Raghavachari, A. Rendell, J. C. Burant, S. S. Iyengar, J. Tomasi, M. Cossi, N. Rega, J. M. Millam, M. Klene, J. E. Knox, J. B. Cross, V. Bakken, C. Adamo, J. Jaramillo, R. Gomperts, R. E. Stratmann, O. Yazyev, A. J. Austin, R. Cammi, C. Pomelli, J. W. Ochterski, R. L. Martin, K. Morokuma, V. G. Zakrzewski, G. A. Voth, P. Salvador, J. J. Dannenberg, S. Dapprich, A. D. Daniels, O. Farkas, J. B. Foresman, J. V. Ortiz, J. Cioslowski and D. J. Fox, *Gaussian 09, Revision B.01*, Gaussian, Inc., Wallingford CT, 2010.
- 56 K. Wolinski, J. F. Hinton and P. Pulay, *J. Am. Chem. Soc.*, 1990, **112**, 8251–8260.
- 57 J. R. Cheeseman, G. W. Trucks, T. A. Keith and M. J. Frisch, *J. Chem. Phys.*, 1996, **104**, 5497–5509.
- 58 M. W. Lodewyk, M. R. Siebert and D. J. Tantillo, *Chem. Rev.*, 2012, **112**, 1839–1862.
- 59 D. Flaig, M. Maurer, M. Hanni, K. Braunger, L. Kick, M. Thubauville and C. Ochsenfeld, *J. Chem. Theory Comput.*, 2014, **10**, 572–578.
- 60 D. Massiot, F. Fayon, M. Capron, I. King, S. Le Calvé, B. Alonso, J.-O. Durand, B. Bujoli, Z. Gan and G. Hoatson, *Magn. Reson. Chem.*, 2002, **40**, 70–76.
- 61 K. Robinson, A. McCluskey and M. I. Attalla, *ChemPhysChem*, 2011, **12**, 1088–1099.
- 62 P. D. Vaidya and E. Y. Kenig, *Chem. Eng. Technol.*, 2007, **30**, 1467–1474.
- 63 J. H. Drese, S. Choi, R. P. Lively, W. J. Koros, D. J. Fauth, M. L. Gray and C. W. Jones, *Adv. Funct. Mater.*, 2009, **19**, 3821–3832.
- 64 R. Serna-Guerrero, E. Da'na and A. Sayari, *Ind. Eng. Chem. Res.*, 2008, **47**, 9406–9412.
- 65 D. Shimon, C.-H. Chen, J. J. Lee, S. A. Didas, C. Sievers, C. W. Jones and S. E. Hayes, *Environ. Sci. Technol.*, 2018, **52**, 1488–1495.

